

See discussions, stats, and author profiles for this publication at: <https://www.researchgate.net/publication/275256104>

Origin of Toughness in Dispersion-Cast Nafion Membranes

ARTICLE *in* MACROMOLECULES · APRIL 2015

Impact Factor: 5.8 · DOI: 10.1021/ma502538k

READS

42

6 AUTHORS, INCLUDING:



[Yu Seung Kim](#)

Los Alamos National Laboratory

114 PUBLICATIONS **5,973** CITATIONS

[SEE PROFILE](#)



[Rex P Hjelm](#)

Los Alamos National Laboratory

118 PUBLICATIONS **1,707** CITATIONS

[SEE PROFILE](#)

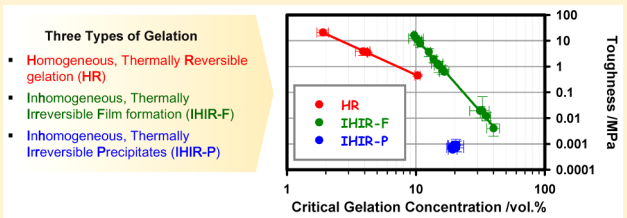
Origin of Toughness in Dispersion-Cast Nafion Membranes

Yu Seung Kim,^{*†} Cynthia F. Welch,[‡] Rex P. Hjelm,[§] Nathan H. Mack,^{||} Andrea Labouriau,[⊥] and E. Bruce Orler[‡]

[†]Sensors and Electrochemical Devices Group, [‡]Polymers and Coatings Group, [§]Materials Science in Radiation & Dynamic Extremes Group, ^{||}Physical Chemistry & Applied Spectroscopy Group, and [⊥]Chemical Diagnostics and Engineering Group, Los Alamos National Laboratory, Los Alamos, New Mexico 87545, United States

Supporting Information

ABSTRACT: The gelation behavior of Nafion dispersions was investigated using small-angle neutron scattering to better understand the mechanical toughness of dispersion-cast Nafion membranes. Three types of gelation were observed, depending on dispersing fluids: (i) homogeneous, thermally reversible gelation that was present in most aprotic polar dispersing fluids; (ii) inhomogeneous, thermally irreversible gelation as films, found in alcohols; and (iii) inhomogeneous, thermally irreversible gelation which precipitates in water/monohydric alcohol mixtures. The mechanical toughness of dispersion-cast Nafion membranes depends on the dispersing fluid, varying by more than 4 orders of magnitude. Excellent correlation between the critical gelation concentration and mechanical toughness was demonstrated with the Nafion membranes cast at 140 °C. Additional thermal effects among Nafion membranes cast at 190 °C were qualitatively related to the boiling point of dispersing fluids. Little correlation between mechanical toughness and percent crystalline area of Nafion was observed, suggesting that the origin of mechanical toughness of dispersion-cast Nafion membranes is due to chain entanglements rather than crystallinity. The correlation between critical gelation concentration and mechanical toughness is a new way of predicting mechanical behavior in dispersion-cast polymer systems in which both polymer-dispersing fluid and polymer–polymer interactions play a significant role in the formation of polymer chain entanglements.



1. INTRODUCTION

Nafion was invented by Walther Grot in the late 1960s¹ and first commercialized as a membrane separator for chlor-alkali cells. During the 1990s, extrusion-cast Nafion membranes were used for a variety of fuel cells and other electrochemical applications. Further demands for better device performance and processing advancement led to the development of dispersion-cast Nafion membranes.² The commercialization of dispersion-cast Nafion membranes in the mid-2000s provided desirable thickness uniformity and improved mechanical properties required for proton exchange membrane fuel cell applications. However, the dispersing fluid effects that impact the mechanical properties of dispersion-cast Nafion membranes are still poorly understood.

Two factors known to impact the mechanical properties of dispersion-cast Nafion are dispersing fluids and thermal treatments. Moore and Martin found that the Nafion membranes cast from water/monohydric alcohol mixtures were brittle, while the Nafion membranes cast from a high boiling point dispersing fluid such as dimethyl sulfoxide exhibited much better mechanical properties and solvent resistance, similar to extrusion-cast Nafion.³ Gebel et al. observed that thermal treatment by annealing at 80–200 °C improved mechanical properties of the cast Nafion membranes compared to lower temperature treatments.⁴ On the basis of wide- and small-angle scattering data, they proposed that the increased crystalline order that occurred from thermal treat-

ment might be related to the enhancement of mechanical properties. Moore and Martin also confirmed that their dispersion-cast Nafion had semicrystalline structure, whereas there was no evidence for crystallinity in cast membranes after low-temperature treatments.⁵ However, several observations contradict this presumption regarding crystallinity,⁶ and Mauritz and Moore later stated that the brittle nature of the recast Nafion was not due to the lack of crystallinity but to the lack of chain entanglement or coalescence between Nafion particles.⁷ While this statement is now believed to be the correct view on the mechanical origin of recast Nafion, there have been no systematic studies to determine the relationships between dispersing fluids, thermal history, and mechanical properties derived from dispersion-cast Nafion.

The importance of Nafion colloidal morphology to the processing and mechanical properties of dispersion-cast membranes was recognized as early as the 1980s, resulting in extensive studies on Nafion morphology in liquid media. Aldebert et al. first proposed the colloidal morphology of Nafion in liquid media.⁸ They observed that the small-angle neutron scattering (SANS) peak for Nafion dispersions in pure water and ethanol was proportional to the inverse square root of the particle volume fraction ($\phi^{1/2}$ law). This trend suggested

Received: December 16, 2014

Revised: March 12, 2015

that Nafion particles in the dispersions are bidimensional (i.e., cylindrical rods) rather than three-dimensional (i.e., spherical particles) or unidimensional (i.e., lamella structure). Further geometrical and Guinier analyses led them to suggest hexagonal packing of rodlike Nafion particles. All observed colloidal particles of Nafion in various dispersions, including aprotic polar dispersing fluids, as well as water/alcohol mixtures, were shown to have cylindrical morphology with various diameters and lengths. Szajdzinska-Pietek et al. suggested another colloidal morphology and aggregation process based on electron-spin resonance studies.⁹ They observed a high degree of order in the Nafion dispersions in water and in formamide. They explained that this structure was formed as a result of physical cross-links between rods, as parts of the outside chains of rodlike Nafion micelles became incorporated into other rods, forming reverse micelles as the concentration of the polymer increased. While the hexagonal packing of rodlike micelles or the network structure of reverse micelles partly explains the mechanical and rheological properties of Nafion, no attempt has been made to correlate the particle morphology and aggregation process with the mechanical toughness of the dispersion-cast membranes.

There has been little progress on systematic studies of dispersion-cast Nafion, partly because of the limited availability of Nafion dispersions and the complexity of the analysis, particularly with multiple dispersing fluid components. Nafion is composed of an extremely hydrophobic polytetrafluoroethylene backbone with perfluorinated pendant chains containing hydrophilic sulfonic acid groups. The differences in polarity between the backbone and sulfonic acid group containing side chains make solvation of the polymer difficult. Most Nafion dispersions are formed after elaborate reprecipitation or replacement processes from an aqueous dispersion.¹⁰ Recently, our research group developed a direct dispersion technique for perfluorosulfonic acid polymers.¹¹ The key process for this technique is hydrothermal treatment and a subsequent low temperature drying process: Nafion membranes are treated in boiling water and dried below the phase-transition temperature,¹² ca. 60 °C. The boiling treatment provides sufficient energy to form hydrated ionic clusters,¹³ and the mild drying process maintains the long-range ordering of polymer backbone. The surface energy of Nafion in the partly dried state is lower than the fully hydrated state,¹⁴ which enables production of Nafion dispersions in a wide range of dispersing fluids without reprecipitation or replacement procedures. Thus, combined with the conventional Grot's high temperature/high pressure processing,¹⁵ this method enables the preparation of numerous Nafion dispersions in pure water, monohydric and polyhydric alcohols, and aprotic dispersing fluids as well as water/alcohol mixtures.

We have discovered that Nafion colloidal morphology in liquid media is much more complex than had been reported,¹⁶ and the durability of proton exchange membrane fuel cells strongly depends on the Nafion morphology in the dispersing fluid that is used for electrode fabrication.¹⁷

This paper correlates the morphological structures obtained by SANS of dilute, concentrated, and gelled Nafion dispersions with the mechanical properties of Nafion membranes obtained from the dispersion-cast process: We report three types of gelation behaviors of Nafion dispersions for the first time, and the morphological features of Nafion dispersions by SANS analysis are addressed in relation with each gelation behavior. Critical gelation concentrations of Nafion dispersions are then

measured in order to correlate the mechanical toughness of the dispersion-cast membranes. The influences of thermal treatment and crystalline structure were also explored in order to discuss the origin of mechanical toughness of dispersion-cast Nafion membranes.

2. EXPERIMENTAL SECTION

2.1. Materials. Commercial Nafion NRE-212 membranes (EW = 1100) were purchased from Ion Power Inc. The acid (H^+) form Nafion membranes were converted to Na^+ form by immersion in boiling 1 wt % solution of NaOH for 90 min and subsequent rinsing with boiling deionized water for 90 min to remove any residual NaOH. The prepared Na^+ form membranes were stored in deionized water until use. All dispersing fluids except water were purchased from commercial vendors. Reagent grade anhydrous methanol, ethanol, 1-propanol, 2-propanol, 1-butanol, acrylonitrile, acetone, dimethylacetamide (DMAc), *N*-methylpyrrolidone (NMP), dimethylformamide (DMF), dimethyl sulfoxide (DMSO), and *N*-methylformamide (NMF) were purchased from Fisher Scientific. Ethylene glycol, 1,2-propanediol, 1,3-propanediol, 1,2-butanediol, 2,3-butanediol, 1,3-butanediol, 1,4-butanediol, 1,2-pentanediol, 2,4-pentanediol, 1,2-hexanediol, 1,2-octanediol, glycerol, and 1,2,4-butanetriol were purchased from Aldrich and TCI America. Millipore deionized water ($R > 18 M\Omega$) was used.

2.2. Preparation of Nafion Dispersion. Nafion dispersions in water, monohydric alcohols, and water/alcohol mixtures were prepared by a conventional high pressure technique in a closed vessel.¹⁵ Typically, 1 g of Na^+ form Nafion membrane with 39 g of dispersing solvent was placed in a 200 mL closed vessel; the solid content was 2.5 wt %. The vessel was heated in a silicone oil bath at 100 °C for 2 h. If Nafion was not completely dispersed in the dispersing fluid, the temperature was increased by 10 °C, and the process was repeated with 10 °C temperature increments until no solid residue remained. Once the approximate dispersing temperature was determined, the minimum temperature to disperse Nafion completely was more precisely determined by repeating the procedure using 2 °C increments from the highest temperature at which Nafion remained undispersed in the previous measurements. We repeated this procedure with 1 °C increments to determine the dispersion temperature.

Nafion dispersions in aprotic and polyhydric alcohols were prepared by the direct dispersion technique.¹¹ Na^+ form Nafion membranes were immersed in boiling water for 90 min and dried at 60 °C *in vacuo* for 2 h. 0.3 g of the pretreated Nafion was placed in a 20 mL vial with 11.7 g of dispersing fluid; the solid content was 2.5 wt %. To determine the approximate dispersion temperature, the vial was placed in a convection oven and heated from 70 °C (for aprotic solvents), 180 °C (for trihydric alcohols), or 110 °C (for other solvents) by 5 °C increments for 1 h. The dispersion temperature was then refined by repeating this procedure with 1 °C increments from the highest "undispersed" temperature. Dispersions for gelation point measurement and for casting membranes were prepared, after double-checking the dispersion temperatures with the above procedures, using 4 g of Na^+ form Nafion and 156 g of dispersing fluid.

2.3. Dispersion Morphology. Small-angle neutron scattering (SANS) measurements were performed on the time-of-flight, Low-Q diffractometer (LQD) at the Manuel Lujan Jr. Scattering Center at Los Alamos National Laboratory. Samples were placed in 1 mm path length fused silica cells. Data were reduced by conventional methods to an absolute scale,¹⁸ of differential scattering cross section per unit volume, $\Sigma(Q)/d\Omega$ (cm^{-1}), as a function of momentum transfer, $Q = 4\pi/\lambda \sin \theta$, where 2θ is the scattering angle and λ is the incident neutron wavelength. Reduced solvent background was subtracted from each sample data set. Fitting of the data was performed with the SANS and USANS Data Reduction and Analysis software (Igor Macros), provided by the NIST Center for Neutron Research.¹⁹

¹⁹F NMR was obtained using a Bruker Avance 300 spectrometer operating at 282.4 MHz. The pulse length was 2.5 μs , and the delay time was 10 s. Spectra were taken using a 4 mm zirconia rotor without

Table 1. Boiling Point (bp) of Dispersing Fluids, Dispersing Temperature (T_{disp}), and Critical Gelation Concentration (CGC) of Nafion Dispersions

dispersing fluid type	dispersing fluid	bp (°C)	T_{disp} (°C)	CGC		gelation type
				wt %	vol %	
aprotic	DMAc	165	76	3.8 ± 0.4	1.9 ± 0.2	HR
	DMF	153	80	7.9 ± 0.5	3.9 ± 0.5	HR
	NMP	204	86	7.9 ± 0.4	4.2 ± 0.2	HR
	DMSO	189	100	17.2 ± 0.7	10.3 ± 0.5	HR
	NMF	183	97	23.5 ± 2.1	13.4 ± 1.3	IHIR-F
alcohol	mono	methanol	65	55.3 ± 0.3	32.8 ± 0.2	IHIR-F
		ethanol	78	28.7 ± 1.2	13.7 ± 0.8	IHIR-F
	diol	ethylene glycol	197	153	34.0 ± 2.8	IHIR-F
		1,2-propanediol	188	121	25.0 ± 1.7	IHIR-F
		1,3-propanediol	214	164	27.3 ± 2.1	IHIR-F
		1,2-butanediol	195	108	19.5 ± 0.1	IHIR-F
		2,3-butanediol	177	114	22.5 ± 1.1	IHIR-F
		1,3-butanediol	207	128	25.5 ± 2.3	IHIR-F
		1,4-butanediol	235	153	27.3 ± 1.2	IHIR-F
		1,2-pentanediol	206	108	18.2 ± 0.4	IHIR-F
		2,4-pentanediol	198	124	19.6 ± 1.1	IHIR-F
	triol	1,2-hexanediol	223	124	19.1 ± 2.2	IHIR-F
		glycerol	290	199	42.1 ± 6.1	IHIR-F
		1,2,4-butanetriol	312	176	48.5 ± 4.9	IHIR-F
water based	water	100	220	34.2 ± 3.9	20.6 ± 2.8	IHIR-P
	1:1 mixture	methanol	100/65	152	32.9 ± 3.0	IHIR-P
		ethanol	100/78	140	32.4 ± 0.4	IHIR-P
		1-propanol	100/97	130	32.4 ± 2.1	IHIR-P
		2-propanol	100/83	124	33.9 ± 4.2	IHIR-P
		1,4-butanediol	100/235	170	23.2 ± 1.0	IHIR-F
		1,5-pentanediol	100/242	177	40.5 ± 2.9	IHIR-F

spinning and a probe with very low fluorine background. ^{23}Na NMR was obtained using a Bruker Avance 400 spectrometer operating at 105.8 MHz. The pulse length was 6.0 μs , and the delay time was 3 s. Spectra were taken using a 4 mm zirconia rotor without spinning. The spectrum of the NaCl solid sample was obtained by spinning the sample at 5 kHz.

2.4. Gelation Behavior. The gelation behavior of the Nafion dispersions was characterized by observing gel formation during dispersing fluid evaporation. In this procedure a 5–30 mL sample of 2.5 wt % Nafion dispersion (taken from the large batch) was placed in an uncapped vial and heated in a convection oven at 140 °C. The dispersions were inspected every 15 min in order to observe the gelation behavior. When the dispersion became a gel, the approximate gelation concentrations were calculated from gravimetric measurements. The critical gelation concentration (CGC, defined as the lowest dispersion concentration that resulted in a stable gel without liquid flow by the vial inversion method) was determined in a second evaporation experiment. Again, a 5–30 mL sample of a given 2.5 wt % Nafion dispersion was placed in an uncapped vial in a convection oven at 140 °C. Dispersing fluid evaporation was allowed to proceed until the Nafion concentration reached a few percent below the approximate gelation concentration. The sample was then quenched to 25 °C in a water bath and then thermally equilibrated for 15 min. The gelled state was then assessed using the inversion test. We repeated this procedure by further evaporation until the CGC point was obtained. The CGC value was obtained on at least three independent samples for each dispersing fluid, and the standard deviation of the CGC values for the independent samples was reported as an error bar.

2.5. Membrane Casting. Nafion membranes were dispersion-cast from 2.5 wt % dispersions in most dispersing fluids at 140 or 190 °C for 6 h. For Nafion dispersions in monohydric alcohols and water/monohydric alcohol mixtures, the membranes were cast at 80 °C for 6 h and subsequently heated at 140 or 190 °C for an additional 6 h. This

two-step procedure allowed for casting of bubble-free membranes with similar thermal history as other membranes. For Nafion dispersions in high boiling point triols such as glycerol and 1,2,4-butanetriol, the membranes were cast at 140 °C for 24 h or 190 °C for 6 h. All cast membranes were then placed in a 50 °C water bath for 30 min to remove any residual dispersing fluids and vacuum-dried at 60 °C for 1 h. The prepared samples were stored in a desiccator prior to mechanical testing and TEM analysis.

2.6. Mechanical Property Measurement. The mechanical properties of all samples were measured within 24 h after drying. The stress-strain properties of the dispersion-cast membranes were measured using a dynamic mechanical analyzer (TA Instruments Q800-RH) using five 30 × 10 mm² (for most samples) or three 10 × 5 mm² (for brittle membranes) rectangular test strips. The temperature of the environmental chamber was increased to 50 °C at 2 °C/min. After equilibrating the samples at 50 °C, 0% RH for 1 h, the tensile measurements were performed at a load ramp of 0.5 MPa min⁻¹. The mechanical properties were obtained on at least three independent samples for each dispersing fluid at two cast temperatures, and the standard deviation was reported as an error bar. The tensile toughness was calculated by integration of the stress-strain area.

2.7. Crystalline Structure Analysis. Transmission electron microscopy (TEM) was used to examine the crystalline structure of dispersion-cast membranes. Dispersion-cast membranes (Na^+ form) were prepared for TEM analysis by embedding in epoxy (Araldite 6005, SPI Supplies) and then sectioning on a Leica Ultra Microtome. For comparison, commercially available Nafion NRE-211 and Nafion 112 (Na^+ form) were prepared for TEM analysis in the same way. The ~50 nm thick sections were transferred to Cu TEM grids and then examined on a Hitachi HF3300 operated at 300 kV. In order to compare the relative difference of crystallinity, percent crystalline areas of each membrane in at least three different positions with 50 nm scale resolution were calculated using image processing software (Icy, v. 1.5.4.2, Institut Pasteur).

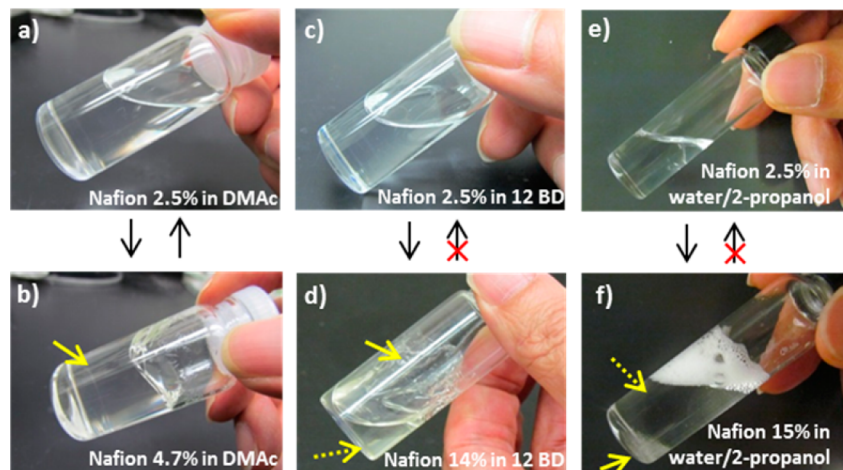


Figure 1. Homogeneous, thermally reversible (HR) gelation (a) sol and (b) gel. Inhomogeneous, thermally irreversible gelation as a film (IHIR-F) (c) sol and (d) partial gel (arrows indicate sol phase (dotted) and film gel phase (solid)). Inhomogeneous, thermally irreversible gelation with precipitation (IHIR-P) (e) sol and (f) partial gel (arrows indicate sol phase (dotted) and precipitate gel phase (solid)).

3. RESULTS AND DISCUSSION

3.1. Dispersion and Gelation Process. Table 1 shows the boiling point (bp) of dispersing fluids, Nafion dispersing temperature (T_{disp}), and critical gelation concentration (CGC) of the dispersions. Nafion (EW = 1100) dispersed in most of the aprotic, alcoholic, and water/alcohol mixture dispersing fluids within the temperature range used, up to ca. 250 °C. Nafion could not be dispersed in pure 1-propanol, 2-propanol, 1-butanol, 1,5-pentanediol, 1,2-octanediol, acetic aldehyde, acetonitrile, or acetone within the tested experimental temperature range.

There were a few noteworthy observations on the dispersion process:

1. The dispersing temperature decreases as the alcohol methyl-to-hydroxyl ratio approaches 2.0. As a result, ethanol ($T_{\text{disp}} = 94$ °C) and butanediol isomers ($T_{\text{disp}} = 108$ –153 °C) have the lowest dispersing temperatures among monohydric and polyhydric alcohols, respectively.

2. The solvents with smaller molecular size have lower dispersing temperatures at a given methyl-to-hydroxyl ratio. For example, methanol ($T_{\text{disp}} = 96$ °C, molar volume: 40.7 cm³) has a lower dispersing temperature than ethylene glycol ($T_{\text{disp}} = 153$ °C, molar volume: 55.8 cm³), which has lower dispersing temperature than glycerol ($T_{\text{disp}} = 199$ °C, molar volume: 73.3 cm³).

3. The dispersing temperature with diols increases with separation of the hydroxyl groups. For example, the dispersing temperature of the butanediol isomers increases from 108 to 153 °C as the distance between the two hydroxyl groups is increased from the 1,2- to the 1,4-position, in spite of the similar Hansen solubility parameters of the isomers (e.g., 28.9–31.3 J^{1/2}m^{-3/2} for butanediols²⁰). A similar trend was observed with pentanediol isomers.

4. Pure water has a relatively high dispersion temperature, ca. 220 °C, and adding alcohols to water lowers the dispersion temperature. For water/2-propanol, the lowest dispersion temperature, which occurred at 102 °C, was observed at a water volume fraction of 0.17 (methyl-to-hydroxyl ratio = 2.0; Figure S1a, Supporting Information). This result is consistent with ¹⁹F NMR mobility measurements of the water/2-propanol dispersions, in which the highest mobility of Nafion backbone and side chains occurred at this same composition.¹⁶ Water/

ethanol dispersions, on the other hand, do not show a minimum temperature but decrease monotonically as the methyl-to-hydroxyl ratio increase to 2.0, i.e., pure ethanol (Figure S1b, Supporting Information).

5. Of all the measured aprotic dispersing fluids, DMAc has the lowest dispersion temperature ($T_{\text{disp}} = 76$ °C). DMF and NMP have intermediate dispersion temperatures ($T_{\text{disp}} = 80$ –86 °C), and NMF and DMSO have higher dispersion temperatures ($T_{\text{disp}} = \sim 100$ °C). Other aprotic dispersing fluids such as acetic aldehyde, acetonitrile, and acetone did not disperse Nafion within the tested experimental temperature range.

The gelation processes of Nafion dispersions were investigated during the evaporation of dispersing fluid. All solvents in their dispersions were evaporated at 140 °C to determine gelation behaviors. Three types of gels were observed: one type is a homogeneous thermally reversible (HR) gel²¹ that forms instantaneously from the sol state at the CGC; the other two types are inhomogeneous and thermally irreversible (IHIR),²² as either a transparent film (IHIR-F) or a white precipitate (IHIR-P). The HR gelation was observed with the Nafion dispersions in DMAc, DMF, DMSO, and NMP (Figure 1a,b). The IHIR gel was observed for the Nafion dispersions in all alcohols, water/alcohol mixtures, and NMF. In the IHIR gelation, partial gelation occurred as the liquid concentrated, and the gel fraction slowly increased with evaporation until all remaining liquid phase disappeared. The IHIR gels did not transform back to the sol-phase upon heating or dilution with the dispersing fluid. The CGC for inhomogeneous gelation was determined as the concentration at which all liquid phase converted to a gel. Below the CGC, the partial gel is either in the form of a film (IHIR-F) or in the form of a white precipitate (IHIR-P). Nafion dispersions in all alcohols (except for the alcohols that cannot make dispersions, e.g., 1-propanol) and in NMF show IHIR-F gelation, e.g., 1,2-butanediol dispersion in Figure 1c,d. Nafion dispersions in pure water or water/monohydric alcohol mixtures show IHIR-P gelation, e.g., water/2-propanol dispersion in Figure 1e,f.

3.2. Colloidal Morphology during Dispersing Fluid Evaporation. The distinctions among gelation processes may be related to the colloidal morphology in dilute dispersion and subsequent polymer particle coalescence during dispersing fluid

evaporation. The NMP, glycerol, and water/2-propanol dispersions go through HR, IHIR-F, and IHIR-P gelation processes, respectively, upon dispersing fluid evaporation. Our previous SANS measurements of 2.5 wt % Nafion in these same dispersing fluids suggested different particle morphologies: NMP, random coil; glycerol, cylindrical particle; and water/2-propanol, large swollen cluster.¹⁶

In this research, we used SANS to examine the change of Nafion dispersion morphology as these dispersing fluids evaporate, as shown in Figure 2. In each case, evaporation

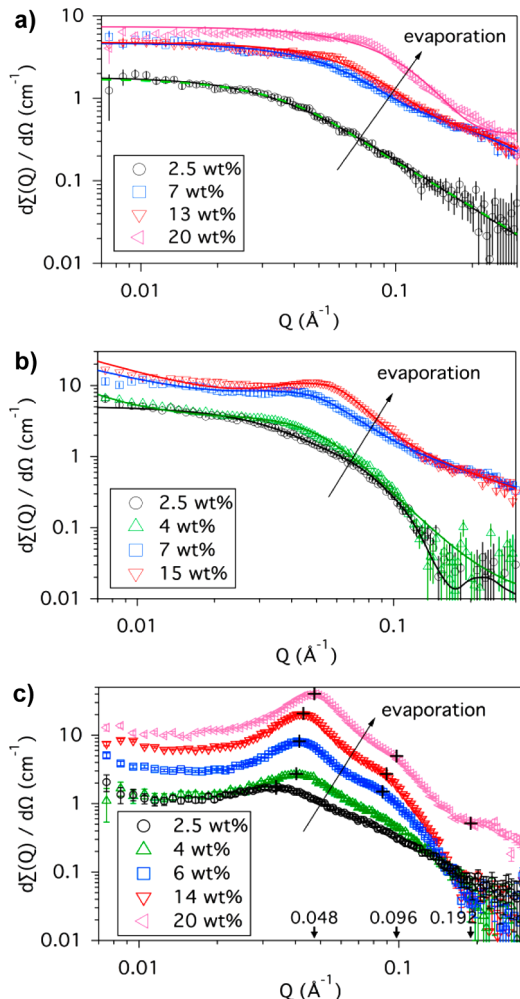


Figure 2. (a) SANS data (symbol) and modeling (line) for the NMP dispersion. All lines except the black solid line: gel network model fit. Black line: Debye form factor fit. (b) SANS data (symbol) and modeling (solid line) for the glycerol dispersion. All lines except the black solid line: Hammouda clustering model. Black line: cylinder form factor model. (c) SANS data (symbol) for the water/2-propanol dispersion. All concentrated dispersions were prepared from 2.5 wt % dispersions by evaporating the dispersing fluid. For (c), the water to 2-propanol ratio changes during evaporation measured from ^1H NMR: 2.5 wt % = 1:1; 4 wt % = 3:1; 6 wt % = 13:1; 14 wt % = 152:1; 20 wt % ≈ pure water.

results in the formation of a shoulder or peak as Nafion concentration increases. Though this type of SANS data can often be modeled by simply including contributions due to the interparticle structure factor ($S(Q)$), none of the curves shown in Figure 2 could be satisfactorily fit with this approach. Furthermore, the SANS curve sets for each dispersion type

(NMP vs glycerol vs water/2-propanol) evolve in noticeably different fashions. The NMP dispersions develop a shoulder in the SANS curves, and this shoulder gradually shifts to higher Q -values. In glycerol, however, a peak develops at 7 wt % Nafion and then shifts to a slightly higher Q -value at 15 wt %. The water/2-propanol dispersion shows a peak even at the lowest Nafion concentration (2.5 wt %); this peak grows in intensity, and higher order peaks develop as concentration increases. These observations suggest that, morphologically, these dispersions evolve quite differently from each other. Thus, each system requires a different approach to modeling the SANS data.

From our previous research, the SANS data from the 2.5 wt % Nafion in NMP dispersion fits well to the Debye form factor for a random coil chain; the model fit yields a radius of gyration (R_g) = 41 Å.¹⁶ From this fit, we can also extract a M_n value of 1.5×10^5 g/mol, which is quite similar to that found by Lousenberg by size exclusion chromatography.²³ While this fit to the Debye form factor suggests that NMP is a theta solvent for Nafion, questions regarding its validity remain, as discussed further below. For the higher concentration NMP dispersions shown in Figure 2a, the data were fit relatively well with a physical gel network that is modeled as a sum of a low- Q exponential decay (e.g., a Gaussian) and a Lorentz-type function at high Q :²⁴

$$I(Q) = I_G(0) \exp[-Q^2 \Xi^2 / 2] + I_L(0) / (1 + Q^2 \xi^2) + B$$

where $I_G(0)$ and $I_L(0)$ are linear coefficients (functional forms are given in ref 24), Ξ represents static correlations in the gel that can be attributed to the solidlike characteristics, ξ is a dynamic correlation length that reflects the liquid nature of the local concentration fluctuations of the gel, and B is the incoherent background, which was fixed at 0.01 cm^{-1} for all of the fits described below. The first term, then, represents a Gaussian distribution of the static cross-links, while the second term describes thermally driven fluctuations due to polymer-dispersing fluid interactions, e.g., in a semidilute dispersion.

Interestingly, the data for the 2.5 wt % NMP dispersion can also be fit to this gel model, and the quality of fit is indistinguishable from that of the Debye form factor fit. The two fits are plotted in Figure 2a, with the solid black line representing the Debye fit and the dotted green line representing the gel model fit. The limiting forms of the two models (Debye form factor and gel network model) are similar; at low Q , $I(Q) \sim \exp(-Q^2 \chi^2)$, and at high Q , $I(Q) \sim -Q^2$. The difference between the two models is the interpretation of the variables, particularly with regard to the argument of the exponential function in the low- Q limit. For the Debye form factor, the Guinier function is recovered in the low- Q limit such that $I(Q) = I_0 \exp(-Q^2 R_g^2 / 3)$. Comparing the argument of this exponential to that of the first term of the gel model (which dominates at low Q), we note that $R_g^2 = 1.5 \Xi^2$; in other words, the correlation length from the gel model fit of 33.4 Å transforms to 40.9 Å, which is the value obtained for R_g from the Debye fit. This result suggests that there are gel particles present that are too large to be detected within the vignette of the SANS measurement; rather, the SANS data reflect the chain structure within the gel particles. Thus, the 2.5 wt % Nafion in NMP dispersion likely consists of microgel particles whose interior structure contains multiple single chains. The gel particles have an open network structure with sufficiently sparse physical network connections such that the SANS signal is dominated by the individual chains.

The trends associated with the gel fit parameters for all four NMP dispersions are shown in Figure 2a (additional modeling details are given in the Supporting Information). The correlation length associated with the static correlations, Ξ , of NMP dispersions decrease as the Nafion content increases, i.e., $33.4 \pm 2.0 \text{ \AA}$ (2.5 wt %), $23.8 \pm 0.3 \text{ \AA}$ (7.0 wt %), $19.7 \pm 0.3 \text{ \AA}$ (13 wt %), and $14.5 \pm 0.1 \text{ \AA}$ (20 wt %). At the same time, the Gaussian scale factor $I_G(0)$ increases over the range of $0.58\text{--}7.0 \text{ cm}^{-1}$. This suggests that as NMP evaporates, more physical cross-links form and the distance between them decreases. The dynamic correlation length, ξ , also decreases with the Nafion content, i.e., $24.3 \pm 3.1 \text{ \AA}$ (2.5 wt %), $6.7 \pm 1.2 \text{ \AA}$ (7.0 wt %), $5.1 \pm 0.3 \text{ \AA}$ (13 wt %), and $1.0 \pm 0.8 \text{ \AA}$ (20 wt %), while the Lorentzian scale factor $I_L(0)$ decreases only slightly, from 1.2 to 0.41 cm^{-1} . The much lower ξ value for the 20 wt % dispersion suggests a highly localized dispersing fluid distribution, probably due to the nanoscale phase-separated morphology induced from the polymer–polymer interaction in the gel state. Such a nanoscale polymer-dispersing fluid inhomogeneity might explain the secondary order feature at ca. 0.18 \AA^{-1} in the SANS data. This feature suggests an additional length scale ($\sim 35 \text{ \AA}$) phase separation, although this structural feature was not accounted for in the model; thus, this feature may account for the noticeably poorer quality of fit to this 20 wt % data set.

The longitudinal osmotic modulus, M_{os} , from the values of $I_L(0)$ was calculated using the equation:²⁴

$$M_{os} = (\rho_p - \rho_s)^2 k T \phi^2 / I_L(0)$$

where ρ_p and ρ_s are the scattering length densities of polymer and solvent, respectively, and ϕ is the polymer volume fraction. Using $\rho_p = 4.2 \times 10^{-6} \text{ \AA}^{-2}$ and $\rho_s = 0.9 \times 10^{-6} \text{ \AA}^{-2}$, we find that M_{os} increases with Nafion concentration, i.e., 0.7 kPa (2.5 wt %) to 5.8 kPa (7 wt %) to 29.6 kPa (13 wt %) to 153 kPa (20 wt %). Thus, the network structure of Nafion chains in the microgel particles of the 2.5 wt % dispersion is extremely weak and possibly a transient one. However, the large values obtained for concentrations above the CGC suggest a strong physical gel, which is consistent with our visual observations.

Further insight into this morphological evolution can be gained through ^{19}F and ^{23}Na NMR measurements, as shown in Figure S2. Narrow peaks are observed for all NMP dispersions (2.5–20 wt %) in the ^{19}F NMR data, indicating high mobility (and a lack of aggregation) of both backbone and side chains at all concentrations, in spite of the changes in physical state (liquid to gel). On the other hand, the broad peaks seen in the ^{23}Na NMR data indicate aggregation of the ionic groups at all concentrations (2.5–20 wt %). Taken together, the NMR and SANS data suggest that insolubility of the ionic groups in NMP drives a local network structure in the gel particles and macroscopic gelation, where the junction points consist of clusters of ionic groups. Indeed, ordering within these ionic clusters may be responsible for the additional feature (not accounted for in the gel model) seen in the SANS data at a Q -value of ca. 0.18 \AA^{-1} .

In glycerol at 2.5 wt %, Nafion formed cylindrical particles with a radius of 22 \AA and length of 150 \AA .¹⁶ The SANS data for Nafion in more concentrated glycerol dispersions were not fit well with the gel network model used for the NMP dispersions; better fits were obtained with the Hammouda clustering model²⁵ (for modeling details, see Supporting Information):

$$I(Q) = \frac{A}{Q^n} + \frac{C}{1 + (|Q - Q_0| \xi)^m} + B$$

For the glycerol dispersions, we interpret this model as follows: the first term describes Porod scattering from clusters of cylindrical Nafion particles, and the second term characterizes the polymer/dispersing fluid interactions, similarly to the Lorentzian term in the gel model used for the NMP dispersions. The prefactors, A and C , take into account the solvation effects present in the cluster. The exponent n is related to the polymer particle/solvent interface of a cluster. The exponent m is related to the geometry of the polymer in the cluster, and Q_0 applies a length scale for polymer inhomogeneity (clumping) within the cluster. For example, $n = 4$ would describe a smooth interface between the Nafion particle cluster and surrounding solvent, and $m = 2$ is consistent with a polymer chain in a theta solvent.²⁵ The remaining parameters are ξ (correlation length) and B (incoherent background, set to 0.01 cm^{-1} for all fits described below).

From the fits shown in Figure 2b (details given in Supporting Information), the prefactor A and exponent n in the Porod term do not change much with concentration. The low magnitudes of the prefactor suggest that the scattering due to clusters is small, perhaps indicating that the number of clusters is small. The SANS data in Figure 2b represent scattering from the liquid phase only. Since the glycerol dispersion follows the IHIR-F process, the clusters may phase separate to the film phase upon reaching a certain size or concentration. The Porod exponent n is low for all three dispersions, with values between 1 and 2. However, the Q -range that is used to determine this exponent is narrow ($Q < 0.015 \text{ \AA}^{-1}$), and the data in that region are noisy; thus, no definite conclusions can be drawn about n . The solvation intensity scale factor, C , changes from 3.5 cm^{-1} (4 wt %) to 5.5 cm^{-1} (7 wt %) to 8.2 cm^{-1} (15 wt %), indicating that the solvation of the Nafion within the particles decreases. Relatively high values of C compared with those of other polymer/solvent systems^{25b} suggest that the dispersing fluid volume fraction in the Nafion particles is low; this is consistent with the form factor modeling of 2.5 wt % glycerol dispersion that shows the volume fraction of glycerol in the Nafion particle is ≈ 0.05 .¹⁶ This result also agrees with the fit results for the Lorentzian exponent m , which are between 2.3 and 3.5, corresponding to poor solvent conditions for polymer chains within the particles.

For 2.5 wt % Nafion in a water/2-propanol mixture (1:1 volume ratio), fitting the SANS data to the large swollen cluster or network model developed by Hammouda²⁵ yields a Porod exponent $n \approx 2$, suggesting that the large-scale clusters ($> 200 \text{ nm}$) are solvent-swollen and have a fuzzy interface.¹⁶ For this water/2-propanol dispersion, 2-propanol is evaporated before the water, as indicated by the water/2-propanol ratio (determined by ^1H NMR) given in the caption to Figure 2. As the Nafion concentration increases during dispersing fluid evaporation, the ionomer network peak at $Q \approx 0.03 \text{ \AA}^{-1}$ shifts slightly to higher Q and grows in intensity, and a shoulder appears in the scattering curve at approximately twice the Q -value of the main peak. At 20 wt %, where there is virtually no 2-propanol remaining in the dispersion, another shoulder becomes evident at approximately 4 times the Q -value of the main peak. These results suggest the formation of an ordered lamellar-type structure of increasing order and decreasing spacing, 195 to 131 \AA , during the evaporation process. The lack of a third-order peak strongly suggests that there is a significant

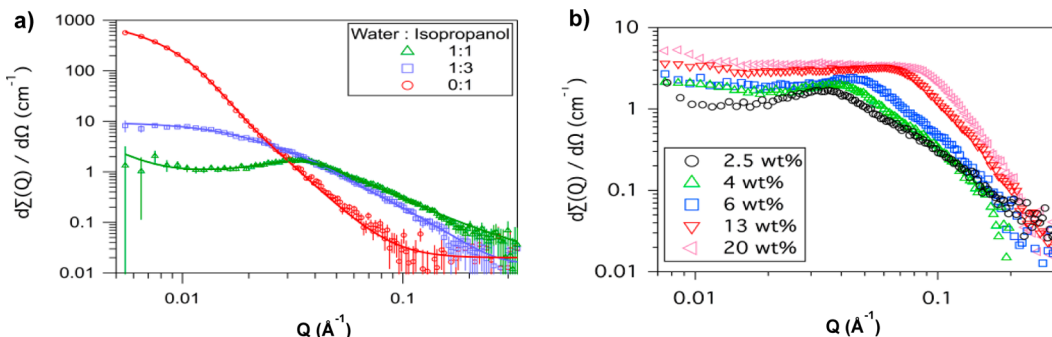


Figure 3. (a) SANS data (symbol) and form-factor modeling (solid line) for the 2.5 wt % Nafion dispersion with varying water to 2-propanol solvent ratios. (b) SANS data (symbol) for water/2-propanol dispersions with varying Nafion concentrations and a fixed 1:1 water to 2-propanol solvent ratio.

change in the scattering length density along the plane of each lamellar layer that is 2/3 of the spacing. For the 20 wt % dispersion, the layer spacing of Nafion lamella structure is 131 Å. Here, we are using “lamellar-type structure” in a broad sense, with the main idea being that there is some type of layering of hydrophilic and hydrophobic domains. Similar scattering curves have been reported for water-swollen films of Nafion and other proton exchange copolymers,²⁶ with the origin of the peaks being attributed to stacked disks or an interconnected network of cylindrical water channels. For our samples, the aqueous phase is the majority phase; thus, an inverted but otherwise similar lamellar-type, two-phase morphology can be envisioned. Regardless of the exact nature of the lamellar morphology, the change in dispersing fluid composition with evaporation is the likely cause for the unique morphological evolution of the Nafion particles from the water/2-propanol binary dispersing fluid system. The effect of such changes in solvent composition can also be observed through ¹⁹F NMR (Figure S3a). Both the backbone and side chain peaks of the 20 wt % Nafion gel prepared from the 2.5 wt % water/2-propanol dispersion are broad, indicating that both the backbone and side chains become less mobile and eventually appear to be unsolvated. ²³Na NMR (Figure S3b) shows that the ionic groups are hydrated (narrow peaks) for the 20 wt % Nafion gel, even though the viscosity of the Nafion gel is high. These NMR data suggest that 2-propanol partitions to solvate the backbone and side chains, while water solvates the ionic groups. As 2-propanol evaporates faster than water, the subsequent changes in the polymer–dispersing fluid interaction drive the morphology from the large-scale cluster particle present in the 2.5 wt % dispersion to a lamellar-type in the concentrated dispersion.

These changes in Nafion morphology observed with evaporation were significantly different from those we observed for 2.5 wt % Nafion dispersions with varying water to 2-propanol ratios (Figure 3a). The form factor fits to the data shown in Figure 3a represent a progression of morphological change with increasing water content: from a polydisperse population of spherical particles at water to 2-propanol = 0:1; to elliptical cylinder at water to 2-propanol = 1:3; and to a highly viscous solution of fuzzy gel-like particles at water to 2-propanol = 1:1 (see Supporting Information for details on these model fits). Note that no lamellar-type morphology evolved for these dilute Nafion dispersions upon varying the water to 2-propanol ratio. To understand more about the concentration effect, SANS experiments were performed for water/2-propanol dispersions with varying Nafion concentrations and a fixed 1:1

water/2-propanol solvent composition. For the preparation of the samples, a 2.5 wt % sample of Nafion in a 1:1 water/2-propanol dispersion was evaporated, but the 1:1 ratio was maintained by gradually adding 2-propanol during the evaporation process. Figure 3b shows that, in contrast to the evaporation process shown in Figure 2c, the peaks at $Q = 0.096$ and 0.192\AA^{-1} are missing. This difference indicates that the Nafion particles in 1:1 water/2-propanol dispersions do not form the lamellar structure as a result of increased concentration. Furthermore, ¹⁹F NMR and ²³Na NMR data show narrow peaks at all concentrations (2.5–20 wt %, Figure S4), as long as the 1:1 ratio of dispersing fluid mixture is maintained; thus, mobilities of the backbone and side chains remains high. Taken together, Figures 2c, 3a, and 3b show that changes in Nafion solubility with increasing water content is likely the reason for the distinct ordering of Nafion to a lamella-type phase for the evaporation process in Figure 2c.

The schematic diagram in Figure 4 shows that the Nafion gel structure depends on the different gelation processes. For HR gelation, the sol-phase contains gel particles. The gel particles contain multiple single chains with loosely connected physical network connections between the polymer single chains. Since the concentration of gel particles must be small, the dispersion allows free flow, i.e., sol state, in spite of the local gelation.²⁷ At the CGC, the Nafion gel particles connect to form a macroscopic gel. The osmotic modulus, M_{os} of the dispersion at CGC, however, is relatively low ca. $M_{os} < 10 \text{ kPa}$, which allows destruction of the network structure upon temperature increase and restoration of the network structure upon temperature decrease; i.e., the gel is thermally reversible. Since the sol–gel transition occurs instantly and homogeneously, the macroscopic sol and gel phases do not coexist. Upon further solvent evaporation, the network structure becomes tighter with enhanced strength. The CGC value of the HR gelation is relatively low compared to CGC of IHIR gelation.

For IHIR-F gelation, the sol phase contains cylindrical Nafion particles, and a swollen film is formed in the gel phase. The CGC value of IHIR-F gelation ranged from 18.2 to 55.3 wt %, depending on the effectiveness of film formation. The cylindrical rodlike geometries of Nafion particles impose constraints on the film forming process, as explored by Abe and Flory.²⁸ However, the rod-like particle structures in the supernatant are not necessarily retained in the gel or film with evaporation, as the components are free to reorganize into the minimum energy for the new phase. Including contributions from an interparticle structure factor ($S(Q)$) for rods gave a

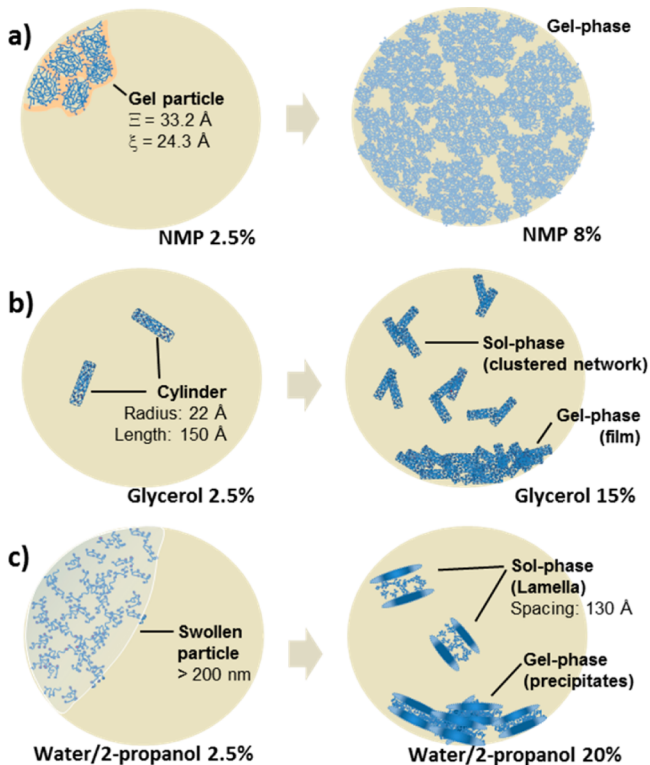


Figure 4. Schematic diagram of Nafion morphology in dilute and concentrated dispersions: (a) NMP dispersion (HR), (b) glycerol dispersion (IHIR-F), and (c) water/2-propanol dispersion (IHIR-P).

poor fit to the SANS data in Figure 2b, suggesting that changes of the dispersion morphology occurs even in the sol phase. Although the detailed film-forming process of IHIR-F gelation is unknown, the following trends were observed regarding the CGC: (i) an insignificant dispersing fluid size effect, e.g., the CGCs of methanol, ethylene glycol, and glycerol dispersions have a similar range, i.e., 31.5–35.8 vol %; (ii) a notable hydroxyl group distance effect, e.g., the CGC value increases from 10.8 to 16 vol % when the dispersing fluid changed from 1,2- to 1,4-butanediols; (iii) a notable alkyl chain length effect, e.g., dispersing fluids with long alkyl chains such as 1,2-pentanediol and 1,2-hexanediol significantly lowered the CGC value by ca. 9.7–10.1 vol %. Note that the dispersing fluid size and methyl-to-hydroxyl ratio effects on CGC have different trends when compared with those on dispersing temperatures. As a result, the methanol dispersion has one of the lowest dispersing temperature yet the highest CGC among other alcoholic dispersions.

For IHIR-P gelation, the sol phase contains swollen Nafion particles and white precipitates formed in the gel phase. The white precipitates in the gel phase should be related to the lamellar-type structure formed in the sol phase of the dispersions. The lamellar spacing within the swollen Nafion particles in water/2-propanol mixtures decreased from 195 to 131 Å, as the solid content increased from 4 to 20 wt %. The faster evaporation rate of monohydric alcohols caused similar CGC values at ~20 vol %. This is reasonable since the gelation of all water/monohydric alcohol dispersions are formed from almost pure water.

Both the IHIR-F and IHIR-P gelation processes, observed in glycerol and water/2-propanol dispersions, respectively, are a result of nonequilibrium dispersion thermodynamics, as

evidenced by the irreversible nature of these gel states. Gelation occurs in these processes when the reduced amount of dispersing fluid cannot maintain the large surface area of the Nafion colloidal particles.²⁹ The physical difference between the gel phases of IHIR-F and IHIR-P, i.e., film vs white precipitate, is likely due to the difference in polymer–dispersing fluid interaction. The dispersing fluids that go through IHIR-F gelation disperse the Nafion relatively well in the form of cylindrical morphology. However, water is not a good dispersing fluid for Nafion, which makes the Nafion particles precipitate instead of making a film. This is supported by the fact that similar white precipitates form in the water/2-propanol dispersions with high 2-propanol content, ca. >90%, where the dispersibility of Nafion was low (indicated by the high dispersing temperature in Figure S1a, Supporting Information). This is consistent with the fact that Nafion cannot be dispersed well in pure 2-propanol.

3.3. Origin of Mechanical Properties of Nafion Membranes.

Our hypothesis is that the origin of the mechanical toughness of dispersion-cast Nafion membranes is the polymer chain entanglements formed during dispersing fluid evaporation. We propose that the morphology of Nafion in the dispersion plays an important role in determining the degree of entanglement in the cast film. We further propose that the CGC is inversely correlated with chain entanglement, and its relationship to tensile toughness will reflect the importance of chain entanglements to film mechanical properties. Likewise, a measure of crystallinity and its correlation with toughness will reflect the importance of Nafion crystal content to mechanical properties. Given the plausible relationship with Nafion dispersion morphology, the degree of chain entanglement is largely related to the chain mobility and time to solidification. While the degree of chain entanglements may be hard to quantify, the CGC must be related to the ease at which chain entanglements can form, as obviously the gel state in these systems must result from physical connections of the polymer. The correlation between the CGC and the chain entanglements may appear to oversimplify the complex process of entanglement involved in film formation followed by the continuous evolution of sintering once the membrane is formed. We provide the connection by reasoning that the thermodynamic and kinetic drivers of polymer–polymer and polymer–dispersing fluid interactions for network formation that allow for lower temperature physical gel formation in a given dispersion system are still active factors as the network coalesces into a highly entangled system with increasing polymer concentration.

Figure 5 shows the tensile toughness of dispersion-cast Nafion as a function of CGC. The tensile toughness, which is distributed over more than 4 orders of magnitude, depends on the type of gelation and has excellent power law correlations with CGC. For the dispersions that showed the HR gelation, the tensile toughness decreased with a power law dependence on CGC of $\alpha = -2.3$, from 21 to 0.45 MPa as the CGC increased from 1.9 to 10.3 vol %. The dispersions that showed the IHIR-F gelation decreased with a larger power law dependence with CGC of $\alpha = -5.7$, with the tensile toughness decreasing from 16.4 to 0.004 MPa as the CGC increased from 9.7 to 40 vol %. Note that the tensile toughness of the Nafion membrane cast from NMF dispersion (an aprotic dispersing fluid that displays IHIR-F gelation behavior) is located near the regression line for Nafion membranes prepared from alcohol dispersions. The water-based dispersions, all of which showed

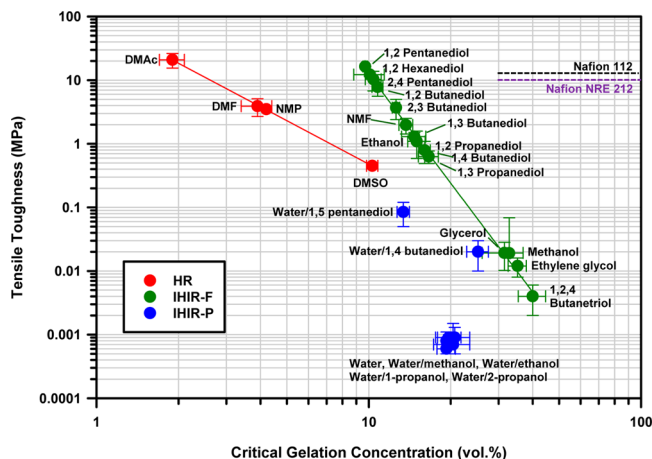


Figure 5. Correlation between tensile toughness and critical gelation concentration. Tensile toughness was measured at 50 °C, 0% RH. Membranes were cast/thermally treated at 140 °C.

an IHIR-P gelation characteristic, did not show a correlation with CGC. The tensile toughness was very low, ca. 0.0008 MPa, and there were no significant differences among samples with different water content, even with pure water with a thermal treatment temperature of 140 °C. The membranes cast from water/polyhydric alcohol dispersions display somewhat higher tensile toughness, ca. 0.02–0.08 MPa, compared to water/monohydric alcohol dispersions. The relatively slow evaporation rate of polyhydric alcohols vs water likely makes an alcohol-rich phase at a later stage of the evaporation process and provides different environments for Nafion chain entanglement as compared with the water/monohydric alcohol mixtures. The power law relationships between tensile toughness and CGC in dispersions with HR or IHIR-F gelation behavior suggest that a lower CGC may provide longer time to form chain entanglements of Nafion. Extremely poor mechanical properties of Nafion membranes cast from water and water/monohydric alcohol mixtures are expected, since water is not a good dispersing agent for Nafion and, therefore, does not provide a good environment for forming chain entanglements.

The difference in power law behavior between the HR and IHIR-F gels is primarily due to the different gelation behaviors. For both dispersions, there must be some degree of chain entanglements occurring at concentrations lower than the CGC. At the point of CGC, the entanglements serve to form a continuous network structure across the entire macroscopic sample. For the dispersions that show the HR gelation behavior, the polymer–dispersing fluid interaction is good,¹⁶ and most chain entanglements begin near the CGC. For the dispersions that show the IHIR-F gelation, polymer–dispersing fluid interactions become too unfavorable compared to polymer–polymer interactions during the evaporation process, so the chain entanglements occur both in liquid (sol) and solid (gel) phases below the CGC. Since the chain entanglements of the IHIR-F type dispersions occur below the CGC, the tensile toughness of the dispersion that shows IHIR-F gelation is always greater than that of the dispersion that shows the HR gelation for a given CGC value.

The effects of chain entanglement on mechanical properties of cast Nafion membranes were further studied by increasing the membrane-casting temperature. Figure 6 shows the plot of mechanical toughness of the Nafion membranes cast at 190 °C

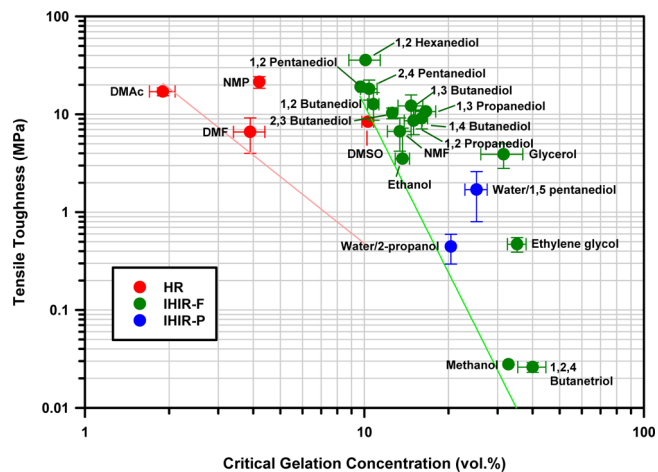


Figure 6. Correlation between tensile toughness and critical gelation concentration. Tensile toughness was measured at 50 °C, 0% RH. Membranes were cast/thermally treated at 190 °C. The red and green lines are the fits generated using the data of Figure 5 for easy comparison with Figure 5 trends.

as a function of CGC. The correlations seen in Figure 5 deteriorated due to the thermal effect. In general, the thermal treatment at 190 °C favors the polymer mobility, the polymer chain entanglements between particles in the dry film, and a better mechanical resistance. As a consequence, most of the samples exhibit a similar toughness around 10 MPa. For the dispersions that show the HR gelation, the tensile toughness of Nafion membranes cast from NMP and DMSO improved significantly, while the tensile toughness of Nafion membranes cast from DMAc and DMF were similar to those cast at 140 °C. Insignificant toughness improvement for the membranes cast from DMAc and DMF dispersions is likely due to the low boiling temperatures of the dispersing fluids (see Table 1), which allow only a limited time for chain entanglement at the high casting temperature. Likewise, the membranes cast from low boiling point alcohols, such as methanol or ethanol, show less improved mechanical toughness, while the membranes cast from high boiling point alcohols (such as 1,2-hexanediol, 1,3-propanediol, 1,3-butanediol, and glycerol) show significantly improved mechanical toughness. The membranes cast from water/monohydric alcohol mixtures also show improved mechanical toughness at the higher casting temperature, in spite of the relatively low boiling point of water. For example, the tensile toughness of water/2-propanol (bp = 100 °C/82.5 °C) increased by more than 2 orders of magnitude, ca. 0.0007 to 0.13 MPa. This may be due to the fact that the high temperature thermal treatment enhances the chain entanglements between particles under a water-rich environment.

The alternate hypothesis that extent of crystallinity determines mechanical toughness of cast Nafion requires correlation between the two measurements. Quantitative analysis of Nafion by wide-angle X-ray scattering (WAXS) is difficult due to the single and broad scattering maximum attributed to the characteristic dimensions within the abundant ionic domains and the fewer crystallites.^{7,30} TEM is another useful tool to compare the crystalline structure of Nafion. However, quantitative determination of crystallinity from two-dimensional TEM images may be difficult. In this research, we examined several spots of the cross section of the dispersion-cast Nafion membranes and recorded three micrographs (50 nm scales) in order to obtain a valid sampling of the film

structure. We then measured the percent crystalline area from the three TEM images to investigate the crystallinity effect. Figure 7 shows representative TEM images of one dispersion-

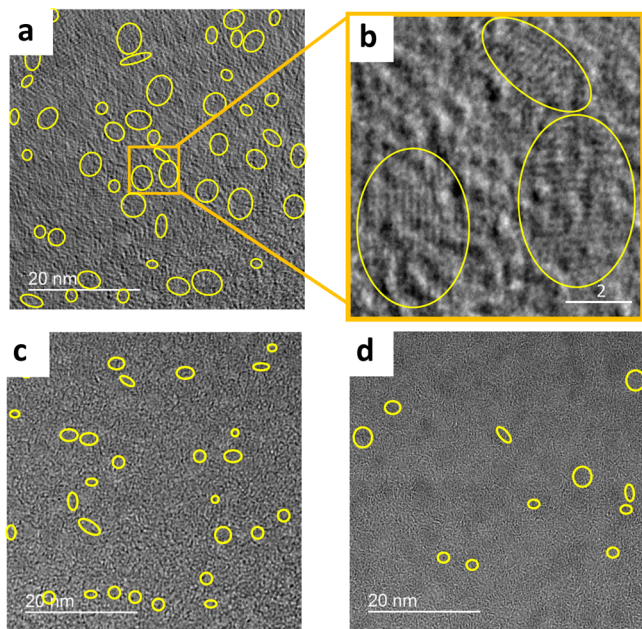


Figure 7. TEM analysis for crystalline structure of Nafion: (a) low and (b) high magnification of Nafion cast from ethylene glycol, (c) commercial Nafion 112, and (d) commercial Nafion NRE-212. All membranes are Na^+ form.

cast and two commercially available Nafion membranes, in which crystalline structures were observed. Figures 7a and 7b are low and high magnifications, respectively, of cross-sectional TEM images for the Nafion membrane cast at 140 °C from ethylene glycol. The low-magnification image shows the distribution and domain size of crystallites as marked in yellow boundaries. The average size of the crystalline domains in these ethylene glycol-cast Nafion membranes was 2.4 nm, which is comparable to the “ionic cluster” size of 1200 EW Na^+ form Nafion found by small-angle X-ray scattering.³⁰ The percent crystalline area calculated through an image analysis was 8.2%. The percent crystallinity values of two other locations of the sample were 7.7 and 9.8%, indicating that there was a notable variation. The high-magnification image shows the crystalline structure of the Nafion membrane. The *d*-spacings (*hkl*) determined from diffractograms of thin sections of the Nafion membranes were 1.9, 2.3, 2.6, 2.7, and 2.8 Å. The *d*-spacing of 2.6–2.8 Å may correspond to (020), as a similar *d*-spacing of 2.7 Å was observed by WAXS for Nafion (EW = 1100) cast from alcohol onto silicon.³¹ The average crystalline domain sizes for commercial extrusion-cast Nafion 112 and solution-cast Nafion NRE-212 (Na^+ form) are similar to that of the Nafion membrane cast from ethylene glycol. The percent crystalline area of the extrusion-cast commercial Nafion 112 was 3.7%, lower than reported crystallinity, ca. 8%.³² The extrusion-cast commercial Nafion 112 has ~2 times more crystalline area than the dispersion-cast commercial Nafion NRE-212, ca. 1.8%, which is consistent with previous WAXS data.³³

The crystalline domain size and percent crystalline area of Nafion membranes cast from different dispersions and two casting temperatures were examined by TEM (Figure S5).

Table 2 summarizes the crystalline domain size and percent crystalline area of the cast membranes. The crystalline domain

Table 2. Crystalline Area and Young's Modulus of Cast Nafion Membranes

solvent	140 °C casting		190 °C casting	
	% crystalline area ^a	modulus (MPa)	% crystalline area ^a	modulus (MPa)
DMAc	7.4 ± 1.6	646 ± 49	4.1 ± 0.8	387 ± 74
NMP	6.8 ± 1.8	684 ± 36	7.9 ± 2.0	450 ± 64
DMSO	3.7 ± 0.7	428 ± 37	NA ^c	417 ± 40
NMF	2.7 ± 0.8	602 ± 61	NA ^c	698 ± 10
ethylene glycol	8.7 ± 1.4	412 ± 43	6.8 ± 1.1	360 ± 35
1,2-propanediol	7.9 ± 2.0	440 ± 50	3.2 ± 1.4	475 ± 26
1,2-pentanediol	6.5 ± 0.6	457 ± 7	7.1 ± 0.8	448 ± 52
1,2-hexanediol	4.5 ± 1.1	536 ± 11	6.5 ± 0.4	515 ± 63
glycerol	7.6 ± 1.6	375 ± 76	11.3 ± 0.8	291 ± 45
water/IPA (1:1)	0.4 ± 0.1	192 ± 20	3.6 ± 1.6	132 ± 18
Nafion NRE-212 ^b	1.9 ± 0.3	623 ± 48		
Nafion 112 ^b	3.7 ± 1.2	668 ± 16		

^aThe errors are sampling standard deviations from three TEM images.

^bMeasured after converting to Na^+ form without thermal treatment.

^cNA = not available.

size is similar among all samples and ranges from 1.3 to 3.5 nm. The crystalline area of the membranes cast from aprotic dispersing fluids ranges from 2.7 to 7.4%. The crystalline area of diols decreased as the methyl-to-hydroxyl ratio increased, indicating that the hydroxyl group plays a certain role in the formation of crystalline structure. For the Nafion membranes cast from aprotic polar or alcohol dispersions, the crystalline area change upon casting temperature is related to the boiling temperature of the dispersing fluid. The crystalline area of Nafion cast from the lower boiling point dispersing fluids, such as DMAc (bp = 165 °C) or 1,2-propanediol (bp = 188 °C), decreases with the high-temperature casting. The decreasing crystalline area with increasing casting temperature for those lower boiling point dispersing fluids is consistent with previous X-ray diffraction results on Nafion cast from DMF (bp = 153 °C): the percent crystallinity of the cast Nafion decreased from 24.4% to 6.0% as the casting temperature increased from 60 to 220 °C.³⁴ In contrast, the crystalline area of the membranes cast from higher boiling point solvents, such as 1,2-hexanediol (bp = 223 °C) and glycerol (bp = 290 °C), notably increased with the high-temperature casting. The membranes cast from intermediate boiling point solvents, such as NMP (bp = 204 °C) or 1,2-pentanediol (bp = 206 °C), had similar crystalline areas (considering the error bounds) under both 140 and 190 °C casting conditions. This is attributed to the slower evaporation rate of high boiling point dispersing fluids, which allows more time for the polymer chains to rearrange. The Nafion membrane cast from water/2-propanol with subsequent thermal treatment at 190 °C had substantially more crystalline area than Nafion treated at 140 °C.

The variation of crystalline area, however, does not explain the difference in mechanical toughness between cast membranes. For example, the tensile toughness of the membranes cast from NMP at 140 °C (crystalline area = 6.8%) is 140 times greater than that of the membrane cast from glycerol dispersion

(crystalline area = 7.6%). In addition, the Nafion cast from 1,2-propanediol at 190 °C (crystalline area = 3.2%) showed more than 10 times greater tensile toughness than the Nafion cast from water/2-propanol at 190 °C (crystalline area = 3.7%). This TEM analysis indicates that the crystalline area of Nafion does not directly impact the mechanical toughness of Nafion membranes. Furthermore, to our surprise, the Young's modulus of the cast membrane does not correlate well with crystalline area. For example, Nafion cast from 1,2-propanediol at 190 °C has less crystalline area but greater modulus compared with Nafion cast from 1,2-propanediol at 140 °C. Another example is Nafion NRE-212, which has the second lowest crystalline area (ca. 1.9%) yet a reasonably high modulus (ca. 623 MPa). Table S1 also shows no direct correlation between the crystalline area and other tensile properties, i.e., the tensile strength or elongation at break. This result is in contradiction with the common intuitive idea that crystallinity plays a major role in the mechanical properties of Nafion.^{6c,35} However, our results are consistent with the recent finding regarding aged Nafion that shows substantial changes in mechanical properties for materials with a constant level of Nafion crystallinity.³³

4. CONCLUSIONS

We investigated the gelation behavior of Nafion dispersions and the origin of mechanical toughness of dispersion-cast Nafion membranes using multiple dispersing fluid systems. The gelation and the colloidal morphology in dilute and concentrated dispersions revealed three distinct gelation processes, depending on dispersing fluid type. Nafion dispersions in most aprotic dispersing fluids underwent homogeneous and thermally reversible (HR) gelation as the ionic groups formed physical cross-links upon dispersing fluid evaporation. Nafion dispersions in pure alcoholic dispersing fluids and NMF underwent inhomogeneous, thermally irreversible gelation with the evolution of a film-forming gel (IHIR-F) until CGC. Nafion dispersions in water/monohydric alcohol mixtures underwent inhomogeneous, thermally irreversible gelation with the formation of an ordered lamellar-type structure in the sol phase and white precipitates in the gel phase (IHIR-P), likely due to the compositional change of water and 2-propanol during evaporation. The effect of dispersing fluids on the mechanical toughness of Nafion membranes is significant, ranging over 4 orders of magnitude, and the Nafion membranes cast from DMAc, 1,2-pentanediol, and 1,2-hexanediol dispersions showed greater mechanical toughness than commercial Nafion NRE 212. Excellent correlations between CGC and mechanical toughness of the cast membranes suggest that polymer chain entanglement induced from polymer-dispersing fluid and polymer-polymer interactions during the evaporation process play a key role in mechanical toughness. The polymer-dispersing fluid interaction alone gauged by the dispersing temperature cannot explain well the origin of mechanical toughness of the cast Nafion membrane. Casting at a higher temperature gave further improvement to the mechanical toughness of the membrane, particularly with high boiling point dispersing fluids and water/monohydric alcohol mixtures. There was no clear relationship between the percent crystalline area and mechanical toughness.

■ ASSOCIATED CONTENT

Supporting Information

Nafion dispersion temperature data, SANS modeling details, ¹⁹F and ²³Na NMR spectra, and TEM images of cast Nafion

membranes. This material is available free of charge via the Internet at <http://pubs.acs.org>.

■ AUTHOR INFORMATION

Corresponding Author

*E-mail: yskim@lanl.gov (Y.S.K.).

Present Address

E.B.O.: Department of Chemistry, Virginia Tech, Blacksburg, VA 24061.

Notes

The authors declare no competing financial interest.

■ ACKNOWLEDGMENTS

This material is based upon work supported by the Department of Energy, Fuel Cell Technologies Program. SANS experiments were conducted at the Low-Q Diffractometer (LQD) beamline of the Los Alamos Neutron Science Center. We thank Drs. Karren More and Perry Kelly (ORNL) for assistance with TEM and X-ray diffractometry experiments. Also, we thank Drs. Kwan-Soo Lee, Baeck Choi, and Christina Johnston (LANL) for sample preparation and useful discussions. Los Alamos National Laboratory is operated by Los Alamos National Security LLC under DOE Contract DE-AC52-06NA25396.

■ REFERENCES

- (1) Grot, W. G. CF=CFCF CF SO F and Derivatives and Polymers Thereof. USP 3718627, 1973.
- (2) Banerjee, S.; Curtin, D. E. Nafion (R) Perfluorinated Membranes in Fuel Cells. *J. Fluorine Chem.* **2004**, *125* (8), 1211–1216.
- (3) Moore, R. B.; Martin, C. R. Procedure for Preparing Solution-Cast Perfluorosulfonate Ionomer Films and Membranes. *Anal. Chem.* **1986**, *58* (12), 2569–2570.
- (4) Gebel, G.; Aldebert, P.; Pineri, M. Structure and Related Properties of Solution-Cast Perfluorosulfonated Ionomer Films. *Macromolecules* **1987**, *20* (6), 1425–1428.
- (5) Moore, R. B.; Martin, C. R. Chemical and Morphological Properties of Solution-Cast Perfluorosulfonate Ionomers. *Macromolecules* **1988**, *21* (5), 1334–1339.
- (6) (a) Werner, S.; Jorissen, L.; Heider, U. Conductivity and Mechanical Properties of Recast Nafion Films. *Ionics* **1996**, *2* (1), 19–23. (b) Zhang, W. J.; Yue, P. L.; Gao, P. Crystallinity Enhancement of Nafion Electrolyte Membranes Assisted by a Molecular Gelator. *Langmuir* **2011**, *27* (15), 9520–9527. (c) Li, J. S.; Yang, X.; Tang, H. L.; Pan, M. Durable and High Performance Nafion Membrane Prepared through High-Temperature Annealing Methodology. *J. Membr. Sci.* **2010**, *361* (1–2), 38–42.
- (7) Mauritz, K. A.; Moore, R. B. State of Understanding of Nafion. *Chem. Rev.* **2004**, *104* (10), 4535–4585.
- (8) (a) Aldebert, P.; Dreyfus, B.; Pineri, M. Small-Angle Neutron-Scattering of Perfluorosulfonated Ionomers in Solution. *Macromolecules* **1986**, *19* (10), 2651–2653. (b) Aldebert, P.; Dreyfus, B.; Gebel, G.; Nakamura, N.; Pineri, M.; Volino, F. Rod Like Micellar Structures in Perfluorinated Ionomer Solutions. *J. Phys. (Paris)* **1988**, *49* (12), 2101–2109. (c) Loppinet, B.; Gebel, G.; Williams, C. E. Small-Angle Scattering Study of Perfluorosulfonated Ionomer Solutions. *J. Phys. Chem. B* **1997**, *101* (10), 1884–1892.
- (9) (a) Szajdzinskapietek, E.; Schlick, S.; Plonka, A. Self-Assembling of Perfluorinated Polymeric Surfactants in Nonaqueous Solvents - Electron-Spin-Resonance Spectra of Nitroxide Spin Probes in Nafion Solutions and Swollen Membranes. *Langmuir* **1994**, *10* (7), 2188–2196. (b) Szajdzinskapietek, E.; Schlick, S.; Plonka, A. Self-Assembling of Perfluorinated Polymeric Surfactants in Water - Electron-Spin-Resonance Spectra of Nitroxide Spin Probes in Nafion Solutions and Swollen Membranes. *Langmuir* **1994**, *10* (4), 1101–1109.

- (10) Silva, R. F.; De Francesco, M.; Pozio, A. Solution-Cast Nafion (R) Ionomer Membranes: Preparation and Characterization. *Electrochim. Acta* **2004**, *49* (19), 3211–3219.
- (11) Kim, Y. S.; Lee, K. S.; Rockward, T. Non-aqueous Liquid Composition of Ion Exchange Polymers. USP 7,981,319, 2011.
- (12) Osborn, S. J.; Hassan, M. K.; Divoux, G. M.; Rhoades, D. W.; Mauritz, K. A.; Moore, R. B. Glass Transition Temperature of Perfluorosulfonic Acid Ionomers. *Macromolecules* **2007**, *40* (10), 3886–3890.
- (13) Zawodzinski, T. A.; Derouin, C.; Radzinski, S.; Sherman, R. J.; Smith, V. T.; Springer, T. E.; Gottesfeld, S. Water-Uptake by and Transport through Nafion(R) 117 Membranes. *J. Electrochem. Soc.* **1993**, *140* (4), 1041–1047.
- (14) Burnett, D. J.; Wood, D.; Kim, Y. S. In Surface Energy Characterization of GDLs and Ionomer Membranes Using Inverse Gas Chromatography at Different Relative Humidity Conditions, 2007 AIChE Meeting, 2007; p 588g.
- (15) Grot, W. G. Process for Making Liquid Compoiston of Perfluorinated Ion Exchange Polymer, and Product Thereof. USP 4433082, 1984.
- (16) Welch, C.; Labouriau, A.; Hjelm, R.; Orler, B.; Johnston, C.; Kim, Y. S. Nafion in Dilute Solvent Systems: Dispersion or Solution? *ACS Macro Lett.* **2012**, *1* (12), 1403–1407.
- (17) (a) Choi, B.; Langlois, D. A.; Mack, N.; Johnston, C. M.; Kim, Y. S. The Effect of Cathode Structures on Nafion Membrane Durability. *J. Electrochem. Soc.* **2014**, *161* (12), F1154–F1162. (b) Kim, Y. S.; Welch, C. F.; Mack, N. H.; Hjelm, R. P.; Orler, E. B.; Hawley, M. E.; Lee, K. S.; Yim, S. D.; Johnston, C. M. Highly Durable Fuel Cell Electrodes Based on Ionomers Dispersed in Glycerol. *Phys. Chem. Chem. Phys.* **2014**, *16* (13), 5927–5932.
- (18) (a) Hjelm, R. P. The Resolution of Tof Low-Q Diffractometers - Instrumental, Data Acquisition and Reduction Factors. *J. Appl. Crystallogr.* **1988**, *21*, 618–628. (b) Seeger, P. A.; Hjelm, R. P. Small-Angle Neutron-Scattering at Pulsed Spallation Sources. *J. Appl. Crystallogr.* **1991**, *24*, 467–478.
- (19) Kline, S. R. Reduction and Analysis of SANS and USANS Data Using IGOR Pro. *J. Appl. Crystallogr.* **2006**, *39*, 895–900.
- (20) Hansen, C. M. *Hansen Solubility Paramters: A User's Handbook*; CRC Press: Boca raton, FL, 2007.
- (21) (a) Loyen, K.; Iliopoulos, I.; Audebert, R.; Olsson, U. Reversible Thermal Gelation in Polymer Surfactant Systems - Control of the Gelation Temperature. *Langmuir* **1995**, *11* (4), 1053–1056. (b) Ka, D.; Seo, M.; Choi, H.; Kim, E. H.; Kim, S. Y. Physical Gelation of Polar Aprotic Solvents Induced by Hydrogen Bonding Modulation of Polymeric Molecules. *Chem. Commun.* **2010**, *46* (31), 5722–5724.
- (22) (a) Lu, P. J.; Zaccarelli, E.; Ciulla, F.; Schofield, A. B.; Sciortino, F.; Weitz, D. A. Gelation of Particles with Short-Range Attraction. *Nature* **2008**, *453* (7194), 499–U4. (b) Kim, Y. S.; Cho, Y. G.; Odkhuu, D.; Park, N.; Song, H. K., A Physical Organogel Electrolyte: Characterized by in Situ Thermo-Irreversible Gelation and Single-Ion-Predominant Conduction. *Sci. Rep.* **2013**, *3*.
- (23) Lousenberg, R. D. Molar Mass Distributions and Viscosity Behavior of Perfluorinated Sulfonic Acid Polyelectrolyte Aqueous Dispersions. *J. Polym. Sci., Polym. Phys.* **2005**, *43* (4), 421–428.
- (24) (a) Horkay, F.; Hecht, A. M.; Mallam, S.; Geissler, E.; Rennie, A. R. Macroscopic and Microscopic Thermodynamic Observations in Swollen Poly(vinyl acetate) Networks. *Macromolecules* **1991**, *24* (10), 2896–2902. (b) Mallam, S.; Horkay, F.; Hecht, A. M.; Rennie, A. R.; Geissler, E. Microscopic and Macroscopic Thermodynamic Observations in Swollen Poly(dimethylsiloxane) Networks. *Macromolecules* **1991**, *24* (2), 543–548.
- (25) (a) Hammouda, B.; Ho, D. L.; Kline, S. Insight into Clustering in Poly(ethylene oxide) Solutions. *Macromolecules* **2004**, *37* (18), 6932–6937. (b) Hammouda, B.; Horkay, F.; Becker, M. L. Clustering and Solvation in Poly(acrylic acid) Polyelectrolyte Solutions. *Macromolecules* **2005**, *38* (5), 2019–2021.
- (26) (a) Nieh, M. P.; Guiver, M. D.; Kim, D. S.; Ding, J. F.; Norsten, T. Morphology of Comb-Shaped Proton Exchange Membrane Copolymers Based on a Neutron Scattering Study. *Macromolecules* **2008**, *41* (16), 6176–6182. (b) Rubatat, L.; Shi, Z. Q.; Diat, O.; Holdcroft, S.; Frisken, B. J. Structural Study of Proton-Conducting Fluorous Block Copolymer Membranes. *Macromolecules* **2006**, *39* (2), 720–730.
- (27) Arleth, L.; Xia, X. H.; Hjelm, R. P.; Wu, J. Z.; Hu, Z. B. Volume Transition and Internal Structures of Small Poly(N-isopropylacrylamide) Microgels. *J. Polym. Sci., Polym. Phys.* **2005**, *43* (7), 849–860.
- (28) Flory, P. J.; Abe, A. Statistical Thermodynamics of Mixtures of Rodlike Particles. 1. Theory for Polydisperse Systems. *Macromolecules* **1978**, *11* (6), 1119–1122.
- (29) Bessling, W. *Conductive Polymers as Organic Nanometals*; Academic Press: New York, 2000; Vol. 5.
- (30) Gierke, T. D.; Munn, G. E.; Wilson, F. C. The Morphology in Nafion Perfluorinated Membrane Products, as Determined by Wide-Angle and Small-Angle X-Ray Studies. *J. Polym. Sci., Polym. Phys.* **1981**, *19* (11), 1687–1704.
- (31) Ludvigsson, M.; Lindgren, J.; Tegenfeldt, J. Crystallinity in Cast Nafion. *J. Electrochem. Soc.* **2000**, *147* (4), 1303–1305.
- (32) Fujimura, M.; Hashimoto, T.; Kawai, H. Small-Angle X-Ray-Scattering Study of Perfluorinated Ionomer Membranes. 1. Origin of 2 Scattering Maxima. *Macromolecules* **1981**, *14* (5), 1309–1315.
- (33) Collette, F. M.; Thominette, F.; Mendil-Jakani, H.; Gebel, G. Structure and Transport Properties of Solution-Cast Nafion (R) Membranes Subjected to Hygrothermal Aging. *J. Membr. Sci.* **2013**, *435*, 242–252.
- (34) Luan, Y. H.; Zhang, H.; Zhang, Y. M.; Li, L.; Li, H.; Liu, Y. G. Study on Structural Evolution of Perfluorosulfonic Ionomer from Concentrated DMF-Based Solution to Membranes. *J. Membr. Sci.* **2008**, *319* (1–2), 91–101.
- (35) Alberti, G.; Narducci, R.; Di Vona, M. L.; Giancola, S. Annealing of Nafion 1100 in the Presence of an Annealing Agent: A Powerful Method for Increasing Ionomer Working Temperature in PEMFCs. *Fuel Cells* **2013**, *13* (1), 42–47.